Pioneering insights into the superior performance of titanium as a fuel in energetic materials

Tao Wu, Vidushi Singh, Baptiste Julien, Christophe Tenailleau, Alain Estève,
Carole Rossi

Pioneering Insights into the Superior Performance of Titanium as a Fuel in Energetic Materials

Tao Wu [a*], Vidushi Singh [a], Baptiste Julien [a], Christophe Tenailleau [b], Alain Estève [a], Carole Rossi [a*]

[a]LAAS-CNRS, University of Toulouse, 7 Avenue du colonel Roche, 31400 Toulouse, France

[b] CIRIMAT, Université de Toulouse, CNRS, Université Toulouse 3 - Paul Sabatier, 118 Route de Narbonne, 31062 Toulouse cedex 9 - France

Abstract

In this work, for the first time, the spotlight was shined on in-depth understanding the reaction mechanism of nanoTi-based thermite. It was found that adding nanoTi into thermite can improve the combustion efficiency and lower the ignition temperature on Al based nanothermites. This experimental study aims at establishing the mechanisms driving this improvement by quantitatively analyzing the oxidation of Ti in contact with a strong oxidizer, such as CuO. Magnetron-sputtered CuO/Ti nanothermites were prepared, partially reacted and characterized using microscopy, differential scanning calorimetry, spectroscopy and X-ray diffractometric. Results show that ~70% of heat of reaction of the Ti/CuO system is released within a single strong exotherm at 430 °C, thus confirming the early and fast Ti oxidation. High resolution electronic microscopy reveals that titania, terminal reaction oxide, is grown and propagates into the Ti layer, driven by the diffusion/reaction of oxygen atoms released by CuO at 300 °C. Spectroscopy measurements show that CuO/Ti redox reaction undergoes a two-step oxidation process: at 300 °C, Ti is first oxidized into TiO and further oxidized into crystalline TiO_2 at 500 °C. This study confirms that Ti can be of great interest in addition or replacement of Al in nanothermites, for applications where it is desirable to lower the ignition temperature. Adding two CuO/Ti bilayers prior to the deposition of CuO/Al multilayers allows decreasing

---

[*] Corresponding author:

  E-mail address: twu@laas.fr (T. Wu), rossi@laas.fr (C. Rossi)

ignition time below the ms (200 µs) against 15 ms without CuO/Ti. Also, a burn rate enhancement factor of ×3, and a reduction of the ignition delay by ×700 is obtained when replacing Al by Ti in standard CuO/Al multilayers.

Keywords: Titanium, nanolaminates, reactive materials, ignition and combustion, thin film

1. Introduction

Thermites are energetic systems consisting of a metal fuel and a metal oxide undergoing a rapid redox reaction associated with a high energy of combustion. Nanothermites refer to as thermites with reactants (fuel and oxidizers) size below 500 nm. As energy-generating materials, nanothermites find applications in material synthesis [1,2], low gas emission heat sources for welding and joining [3–6], initiation [7–9], and also on chip actuations [10–13]. Al fuel is by far the most employed metallic fuel because of its high oxidation enthalpy and low cost, despite the negative impact of the native alumina (Al_2O_3) coated on aluminum which penalizes the ignitability. As for some applications, is desirable to lower the ignition temperature, much research effort is dedicated to the increase of Al ignitability and decrease of its ignition temperature. For example, Williams and Pantoya [14] modified the Al particles reactivity by modifying the $Al-Al_2O_3$ core-shell microstructure through annealing and quenching of the powder, to vary interfacial strain and associated stress. Correlation between altering the Al microstructures by stress and lowering ignition point was also observed in [15,16]. It was also explored in multilayered Al/CuO thermite by Julien and Rossi [17] to tune the ignition point of micro-initiation chip. Others explored the replacement or modification of the native Al_2O_3 passivation layer using metal-organic frameworks [18–20], graphene oxides [21], PVDF [19,22], ZnO [23]. Modifying the Al/Oxidizer interfacial layer is shown to regulate reaction progress by regulating mass transport through it, which is also a key factor to control the ignition point.

Considering other fuels of interest (Boron [24–26], Silicon [27], Magnesium [28], Zirconium [29], Titanium [30], Tantalum [21], see **Fig. S1**) with Al is another effective solution to improve ignitability and combustion performance of nanothermites. Shoshin and Dreizin investigated the ignition temperature of Al–Ti alloys and found that the ignition temperature decreased from 1877 °C (for neat Al) to 969 °C (for a $Al_{0.75}Ti_{0.25}$ alloy) [31]. More recently, Zachariah and coworkers added Ti nanoparticles into various thermites (Si/$KClO_4$ [27], B/CuO [25], Al/I_2O_5 [30]) and the results demonstrated, in certain conditions, a better combustion efficiency and reactivity, i.e., pressurization and burn rate increased by factor ~3 to 6 when 40% of nanoTi is added in B/CuO. Authors suggested that the performance enhancement upon Ti particle doping is due to the intermixing of both boron and titanium particle shells (namely TiO_2 and melting B_2O_3) creating a non-liquid interfacial pathway for a more direct diffusion route for oxygen atoms. In turn, the reaction of oxygen with Ti promotes a higher flame temperature enhancing the melting of boron and volatilization of B_2O_3. These experimental findings not only point to the complexity of the mechanisms governing ternary thermites reactivity but also raise the question of the exact role of the Ti reaction with CuO in such thermite composites, which is poorly documented from a fundamental standpoint.

The objectives of this study are (1) to confirm the ignitability and combustion performance improvement of a Ti-based thermite compared to its Al-based counterpart, and, (2) to understand the mechanisms driving this improvement by quantitatively analyzing the reaction of oxidation of Ti in contact with CuO.

To do so, we employed magnetron-sputtering to grow high purity and well-defined Ti/CuO nanothermite. Contrary to powdered nanothermites in which a thick titania oxide shell layer separates its pure fuel Ti core from the outer surface oxidizer particle, magnetron-sputtered technique permits a very well controlled interface (in thickness and structure) between the fuel and oxidizer. This provides an ideal model-system to quantitatively describe the TiO_x interfacial

oxide growing using a host of characterization techniques including microscopy, thermal analysis, spectroscopy and X-ray diffractometric. CuO was chosen as the oxidizer due to its relative stability in ambient conditions, its ease of sputter-deposition, and its known use as a oxidizing agent/oxygen source for thermite reactions.

Interestingly, we found that oxygen self-diffusion through titania growing interfacial layer is several orders of magnitude larger than that of alumina at low temperatures (< 500 °C) which explains why Ti-based multilayers react most readily. At a similar initiation temperature, the Ti-based sample supports more oxygen transport, thus a greater number of elementary exothermic reactions, causing a greater amount of heat per unit volume. In turn, this drives the system into the self-sustaining reaction mode where sufficient energy is present to activate mass transport across the continuously forming terminal oxide until the reaction is completed. Finally, this technological study provides perspectives for tailoring the ignitability of Al/CuO reactive thin films used in micro-initiation chips [32]. Adding a few Ti nanolayers in the first CuO of Al/CuO multilayers ensures a better ignitability: the initiation of a 8 µm thick Al/CuO energetic film with 2 CuO/Ti bilayers requires 0.3 ± 0.1 mJ against 85 ± 25 mJ without Ti.

2. Materials and methods

2.1. Materials and samples preparation

CuO, Ti, and Al layers were deposited using direct current (dc) magnetron sputtering from Cu, Ti, and Al targets (8 by 3 square inches and ¼ inch thick) using a base pressure of 10^{-7} mTorr in an equipment from Thin Film Equipment (TFE), Italy. For CuO nanolayers, the oxygen and the argon flows were adjusted to 16 and 32 s.c.c.m. resulting in a chamber pressure of 8 mTorr. The sputtering parameters are summarized in **Table S2**. Each sample was cooled to the ambient temperature at the end of the deposition process.

Several multilayer stacks composed of CuO/Ti and CuO/Al bilayers were prepared to ascertain the ignitability (ignition delay/energy) and energetic properties (heat of reaction and burn rate).

For ignition experiments, 5-bilayers of CuO/Al and CuO/Ti were sputter deposited through a patterned shadow mask (5.6×6.7 mm^2 thermite surface area) onto a glass substrate. Titanium filaments were patterned, underneath the nanolaminate line, to resistively heat the multilayer to ignition [33] **(Fig. S2a).** For energetic properties characterization (combustion tests and thermal analysis), 5-bilayers foils made of CuO/Ti and CuO/Al bilayers were fabricated using photolithography and lift-off processes as shown in **Fig. S2a**.

For all the samples, the thicknesses of CuO, Ti and Al were set to 200 nm, 170 nm and 200 nm respectively. This corresponds to 2:1 Al:CuO and Ti:CuO mass ratios (fuel-rich configuration), to be in accordance with previous works [17,33–35]. In addition to the 5-bilayer stacks, trilayers, CuO/Al/CuO and CuO/Ti/CuO, were prepared on a Si substrate to perform for the structural and the interfacial analysis.

Table 1. *Summary of sample preparation and the associated metrological parameters*

Label	# of bilayers	Substrate	Metrology
CuO/Ti; CuO/Al	5; 5	None	Heat of reaction (ΔH_{reac}), Burn rate
CuO/Ti; CuO/Al	5; 5	Glass	Ignition delay/energy
CuO/Ti/CuO/Al	-	Si	Microstructural and interfacial changes

2.2 Characterization

The crystallographic structure of the materials was characterized using a SIEFERT XRD 3000 TT X-Ray diffractometer (XRD) with Cu-Kα radiation ($\lambda = 1.5406$ Å) fitted with a diffracted beam graphite monochromator. The 2θ X-Ray diffractogram was collected from 20° to 60°. The morphological and interfacial analysis of the multilayers were carried out by

Transmission Electron Microscopy (TEM), Scanning Transmission Electron Microscopy (STEM) using a JEOL cold-FEG JEM-ARM200F operated at 200 kV (energy resolution 0.3 eV) equipped with a probe Cs corrector reaching a spatial resolution of 0.078 nm. Elemental distribution and elemental mapping were obtained by energy-dispersive X-ray Spectroscopy (EDX) recorded on a JEOL CENTURIO SDD detector. Chemical composition of the interfacial layer were analyzed by electron energy-loss spectroscopy (EELS) obtained on a Gatan Imaging Filter Quantum using a dispersion of 0.5 eV/channel, a collection semi angle of 19.4 mrad and a convergence semi-angle of 14.8 mrad. The spatial resolution was estimated at 0.5 nm. STEM samples were prepared by Focused Ion Beam (FIB) technique on FEI Helios NanoLab DualBeam.

The heat released during the reaction of each multilayer is characterized via thermal analysis using a Differential Scanning Calorimetry (DSC) performed in Ar atmosphere on a NETZSCH DSC 404 F3 Pegasus system. The scan, normalized to the foil mass (~5 mg), was performed at a constant heating rate of 10 °C.min^{-1} up to 950 °C in Ar atmosphere. After cooling down to room temperature, the sample was reheated with the same process, and the reheating curve was used to correct the baseline of the first heating process. The integrated peak area of DSC curves indicates the heat release of the specific exothermic peak.

For the ignition experiments, a DC current pulse was sent through the Ti filament to achieve ignition resistively. It should be noted that, for each test, the dc current was set according to the resistance value to consistently obtain the same dissipated power of 10 W. A VISHAY, BPV 10 photodiode, diagonally placed ~10 cm from the device and externally biased at 5 V was used to obtain the ignition delay by detecting the optical flash from each ignition test. The photocurrent was recorded through a 1 kΩ resistance. An oscilloscope was used to acquire all the signals during the tests and treated with homemade programs. Several tests were performed for each sample to determine the ignition delay and statistical values are reported. The ignition

energy was determined by calculating the power integral over time recorded from each test. The power is obtained from the temporal record of current and voltage signals registered by the oscilloscope.

The combustion experiments were performed using a flame torch igniting about 50 mg of thermite foils loosely placed on a $30 \times 1 \times 1$ mm^3 poly(methyl methacrylate) (PMMA) trench. The flame propagation was imaged with a high-speed camera (25 cm) (Phantom VEO710L-18GB-M, USA) at 48,000 frames.s^{-1} and a resolution of 512×64 pixels. Around three burn rate experiments were carried out per sample configuration and all the experiments were performed in a constant-pressure air atmosphere. An average burn rate was then calculated by tracking the distance travelled by the reaction front as a function of time by Phantom Camera Control software (three positions in the flame front were used for each burn rate experiment and then an average value was obtained). The experimental benches for ignition and combustion tests are shown in **Fig. S2b** and **Fig. S2c,** respectively.

3. Results and discussion

3.1. Enhanced reactivity of CuO/Ti compared to CuO/Al

Fig.1a and **1b** compare the measured burn rate and ignition delay of CuO/Ti and CuO/Al in ambient condition. The burn rate of CuO/Ti is 3 times faster than CuO/Al. CuO/Ti demonstrated 100% ignition success with a delay of ~ 0.02 ms that is 3 orders of magnitude smaller than CuO/Al (~ 15 ms), giving also 100% of ignition success. Noteworthy the 5-bilayers CuO/Al on glass struggle to sustain continuous propagation, therefore only ~ 10% of the thermite surface area propagates upon ignition, against 100% for 5-bilayers CuO/Ti as shown in **Fig. S3**, which is another indication of the higher reactivity of the CuO/Ti system. **Fig. S4** gives snapshots of the ignition sequences. Overall, ignition and combustion results clearly indicate that CuO/Ti multilayers are much more reactive than CuO/Al ones.
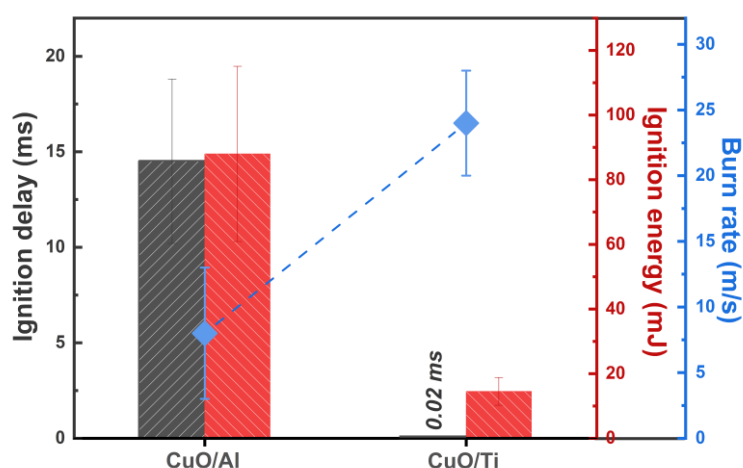
***Figure 1.** Ignition delay/energy and burn rate of CuO/Ti compared to CuO/Al. Samples are composed of 5-bilayers of each reactants with a mass ratio of fuel over oxidizer at 2.*

In order to further investigate the mechanisms of reaction between Ti and CuO responsible of this improvement, thermal behavior of CuO/Ti foils was characterized at slow heating rate and compared to CuO/Al. **Fig. 2** plots the specific heat flow measured by DSC from the ambient temperature to 950 °C for CuO/Ti. DSC plot of CuO/Al multilayers is added to serve as reference. The heats of reaction corresponding to each exothermic event, including the broad bumps are noted as they provide interesting information even though the data must be carefully analyzed as they are highly dependent on the baseline.

The most striking feature of DSC analysis is that CuO/Ti reaction features one single major exotherm located at ~ 430 °C, labelled as peak #1 in **Fig. 2**. This corresponds to the temperature of the first weak and broad exotherm characterizing the CuO/Al reactions in fully dense thermite such as multilayers [33,36,37] and attributed to the dual solid phase diffusion of Al and O atoms released from CuO through the naturally grown interface into the adjacent layers. To elucidate details about the processes observed by DSC, a 2-bilayer CuO/Ti on Si-wafer was heated to intermediate temperatures (300, 500 °C) making sense from the DSC exotherms, recovered, and analyzed by XRD. When annealed to 300 °C, Ti, CuO and Cu_2O are detected, while to 500 °C, TiO_2, Cu_2O and Cu were detected (**Table 2** and **Fig. S5**). This confirms that,

upon heating up, CuO decomposes into Cu_2O. At this stage of annealing, i.e. at 300 °C, the released oxygen atoms may be stored or simply transported through the interface layer to initiate the reaction. As no clear exotherm is seen from the DSC before 300 °C, we can expect slow migration of atoms interacting with Ti in poor quantity that could explain the pre-peak observed at 213 °C. Note that as no TiO_x peak is seen from XRD due to its amorphous nature, so that it is impossible to strongly argue on this early Ti oxidation.

After thermal treatment at 500 °C, copper oxide continues decomposing into Cu_2O, but also in Cu, resulting in a continuous oxidation of titanium in this temperature range. The crystallization of a probably thicker TiO_2 layer, as observed from the XRD curve, corroborates the DSC exotherm where reaction stops, which might result from the crystallization/thickening of TiO_2 inhibiting further migration of oxygen atoms.

Table 2. *Summary of XRD analysis results of CuO/Ti at various temperatures (diagrams are provided in SI)*

Annealing temperatures	Ambient	300 °C	500 °C	950 °C
Constituents	Ti, CuO	Ti, CuO, Cu_2O	Cu_2O, Cu, TiO_2	Cu_2O, Cu, TiO_2

Also, whereas the strongest exothermic reactions in CuO/Al multilayers began just after 550 °C, i.e., just prior to the Al melting (peak # 2 and peak # 3 in **Fig. 2**), CuO/Ti multilayer releases 70% of the total heat of reaction at low temperature (< 500 °C). The high-temperature weak exotherm of CuO/Ti (peak # 2) would be corresponding to a continuation of Ti oxidation due to the higher melting point of titanium (1665 °C, Al being 660 °C).

Table 3 presents the total heat release, ~1580 and ~1187 J/g, for CuO/Al and CuO/Ti respectively, which are for both roughly 50% of their theoretical values (3300 and 2450 J/g, respectively). The typical lower than expected heat release from the foils are usually attributed to the incomplete reaction as sputtered-deposited as CuO is highly defective, as well as heat

losses into the environments. The presence of Cu_2O in post-DSC products confirms the incompleteness of the Ti+CuO. Indeed, XRD analysis of the (**Table 2 & 3** and **Fig. S6**) shows metallic Cu, TiO_2 and Cu_2O signatures in the combustion products. Note that the absence of metallic titanium implies that all Ti has been oxidized to some lower level of oxidation states.

Interestingly, a weaker exothermic peak is detected between 600 and 700 ºC in CuO/Al samples. It can be attributed to the formation of intermetallic Al_2Cu, but also to the further oxidation of aluminum, as these are the two events compatible with this temperature range. XRD analysis (**Fig. S7**) of CuO/Al samples collected from DSC in this region shows: Al, CuO and Cu_2O at 600 °C, indicating that there are still lots of active reactants left for further reaction upon heating at 700 °C, where the dominating component is Al_2Cu with other minor materials such as Cu_2O, Al_2O_3, Cu and Al.

In contrast, no trace of copper-titanium alloy is detected for CuO/Ti measurements after high temperature annealing (950°C).
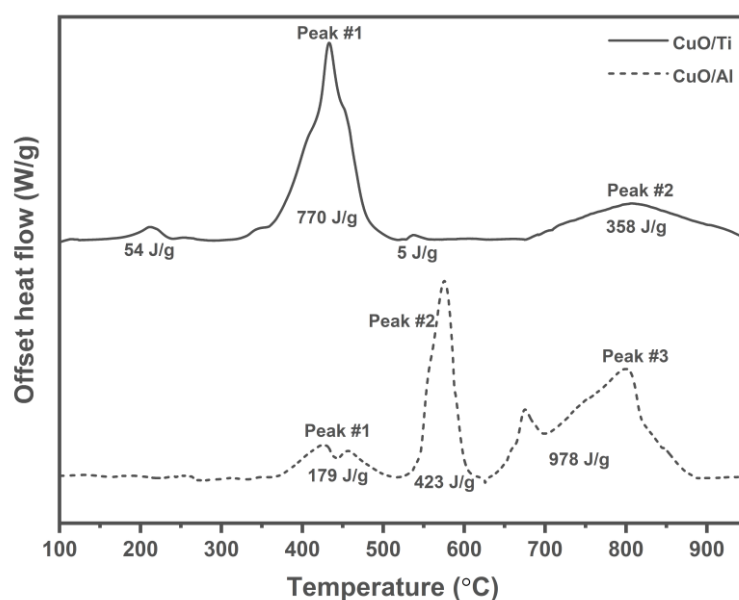

Figure 2. *DSC traces of CuO/Al and CuO/Ti foils in Ar. Foils are composed of 5-bilayers of each reactants with a mass ratio of fuel (Al or Ti) over CuO at 2. Heating rate at 10 °C.min^{-1}.*

Table 3. *Summary of the heat releases from CuO/Al and CuO/Ti foils composed of 5-bilayers. Mass ratio of fuel (Al and Ti) over CuO is fixed at 2.*

Samples	Heat release ($J{\cdot}g^{-1}$)		
	< 500 ºC	Total	Theoretical total
CuO/Al	179	1580	3300
CuO/Ti	824	1187	2450

Thermal analysis suggests that the high reactivity of CuO/Ti multilayers is due to the fast Ti oxidation at low temperature, thus producing a TiO_x growing interface which appears to be a poor barrier to reactant diffusion when comparing it with the amorphous alumina grown in CuO/Al system [36]. With its crystallization at 500 °C, this layer offers a good barrier to mass transport until temperature above 700-900 °C is reached. However, the question of the nature of diffusing reactants, i.e. both Ti and O or only O, is not answered.

Since no Ti/Cu alloying is observed and as the melting point of the titanium is much higher than aluminum, 1665 ºC *vs* 660 ºC, we expect that only atomic oxygen, rather than titanium migrates from CuO to the titanium reservoir. To further analyze the relevance of this conjecture, high resolution microscopy is conducted on CuO/Ti/CuO/Al sample composed of only four nanolayers, to quantitively describe structural and chemical evolution of the TiO_x interfacial layer upon heating. The target temperatures for annealing were set at 300 °C and 500 °C as a result of the DSC analysis, wherein the first CuO/Ti exotherm are observed just after 300 °C and is completed when reaching 500 °C.

3.2. Morphology and chemical analysis of growing interfaces in CuO/Ti *vs* CuO/Al

3.2.1. As deposited

The **Fig. 3a-b** (TEM images and EDX mapping), the CuO/Ti/CuO/Al sample show the four nanolayers: from the bottom to the top, CuO, Ti, CuO, and Al, with thickness of 194 ± 1.2 nm,

161 ± 1.9 nm, 199 ± 1.7 nm, and 200 ± 1.5 nm, respectively. TiO_x nanolayer, can be distinguished on both the EDX maps (**Fig. 3b**) and high magnification TEM images (**Fig. 3c-d**) of the CuO-Ti and Ti-CuO interfaces. Note that throughout this paper A-B refers to an interface formed upon the deposition of B on A. TEM images of CuO-Al interfaces are given in **Fig. S8** as they were detailed in a previous paper [33]. **Table 4** summarizes the thickness and some qualitative information about each interface.

The CuO-Ti interface formed upon Ti sputtered deposition onto the rough CuO surface is overall ill-defined and inhomogeneous, due to the typical roughness of columnar CuO, with an average thickness of 9 ± 2 nm, more than twice thicker than that of CuO-Al interface (4.2 ± 0.7 nm) formed upon the deposition of Al onto CuO. The interface formed upon the CuO sputter-deposition onto Ti (Ti-CuO) is flat and features a thickness of 5.1 ± 0.3 nm, again thicker than that of Al-CuO, 3.8 ± 0.1 nm. The thicker initial interfacial layers in CuO/Ti system compared to CuO/Al plaids for a higher reactivity of Ti as fuel, which also agrees with the higher Ti-O bond energy compared to Al-O (668 kJ.mol^{-1} versus 500 kJ.mol^{-1}). The asymmetry of Ti-CuO and CuO-Ti interfaces observed in TEM images is confirmed by the EDX chemical profile across both interfaces. A quantitative map can be obtained from the EDX spectra and the elemental profile with the atomic percentage across the layers and interfaces permit to qualitatively evaluate the interface chemical composition (**Fig. 4**).
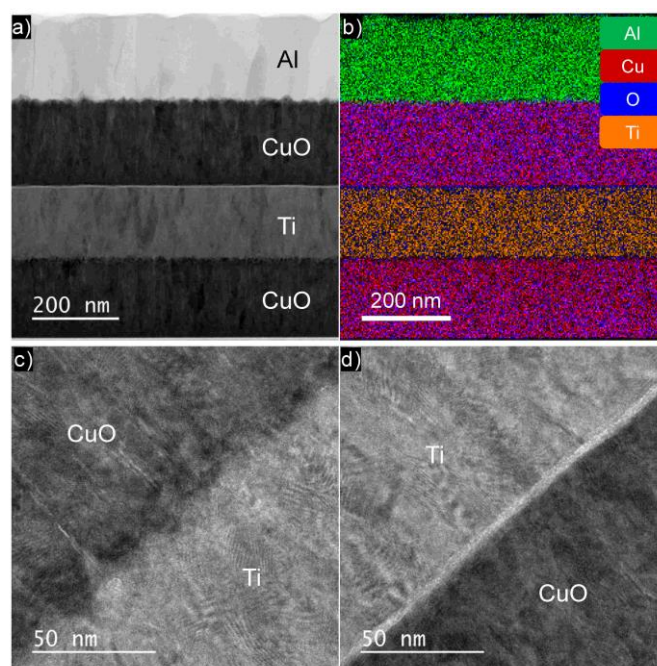
Figure 3. *(a.) TEM micrographs of the cross section of CuO/Ti/CuO/Al sample. (b) corresponding EDX mapping. High magnification TEM micrographs across the two different interfaces (c) CuO-Ti and (d) Ti-CuO. Each color indicates the different elements.*

Table 4. *Summary of measured thicknesses of each layer in untreated CuO/Ti/CuO/Al stack.*

Temperature (ºC)	Measured thickness (nm)							
	CuO	TiO_x	Ti	TiO_x	CuO	Al_xO_y	Al	All
25	194 ± 1	9 ± 3	161 ± 2	5 ± 0	199 ± 2	6 ± 1	200 ± 2	773 ± 3

Across the $CuO/TiO_x/Ti$ interface (**Fig. 4a,** scanned depth from 0 to ~34 nm), the EDX-line scanned profile (**Fig. 4b**) gives a Cu to O atomic ratio very close to 2 in the CuO region in contact with the interface, which implies the as-deposited copper oxide material has reduced to Cu_2O even prior to ignition, i.e., as a consequence of Ti exposure during deposition. However, it is interesting to note that compared to previous result on CuO-Al [33,36], much more oxygen (nearly 15% more) originated from copper oxide is consumed by incoming Ti. The oxygen in CuO content has reduced from ~40% in CuO-Al to ~25% in CuO-Ti (in atomic percentages). It has to be noted that EDX is not really suitable to quantify light elements like O but it can

detect the presence of oxygen with concentrations higher than 10%. For O concentration lower than 10%, we can consider that we reach the limit of detection.

As for the CuO-Ti interface (from 34 to 47 nm in depth), **Fig. 4b** shows there is severe intermixing of Ti, Cu and O with atomic percentages of $34 \pm 23\%$, $44 \pm 23\%$ and $22 \pm 4\%$. It seems the oxygen content remains roughly the same across this interface, while both titanium and copper content undergo drastic changes with crossing over at the average center of the interfacial TiO_x layer. Whereas all three species are present across the whole interface; no single TiO_x phase was identified based on the EDX profile. In the titanium layer, a very small amount of oxygen signal ($< 5\%$) were picked up by EDX and later confirmed by EELS to be background noise.

In the Ti-CuO interface (**Fig. 4c-d**, from ~20 to 35 nm in depth), the oxygen content increases rapidly in the first ~5 nm, where the Ti to O atomic ratio is close to 1.3. This ratio unambiguously defines a TiO layer presence in Ti-CuO interface. Since the deposition of CuO requires O_2 plasma inside the chamber, the fresh-deposited titanium layer is likely to be oxidized by the oxygen prior to CuO deposition. From 25 nm in depth and before Ti disappearances at 35 nm, an intermixing of three species is present, as for the CuO-Ti case. Beyond 35 nm in depth, the Cu and O content stabilize and gives a Cu to O atomic ratio close to 1 within the SNR variation, similar to the Al-CuO case [33].
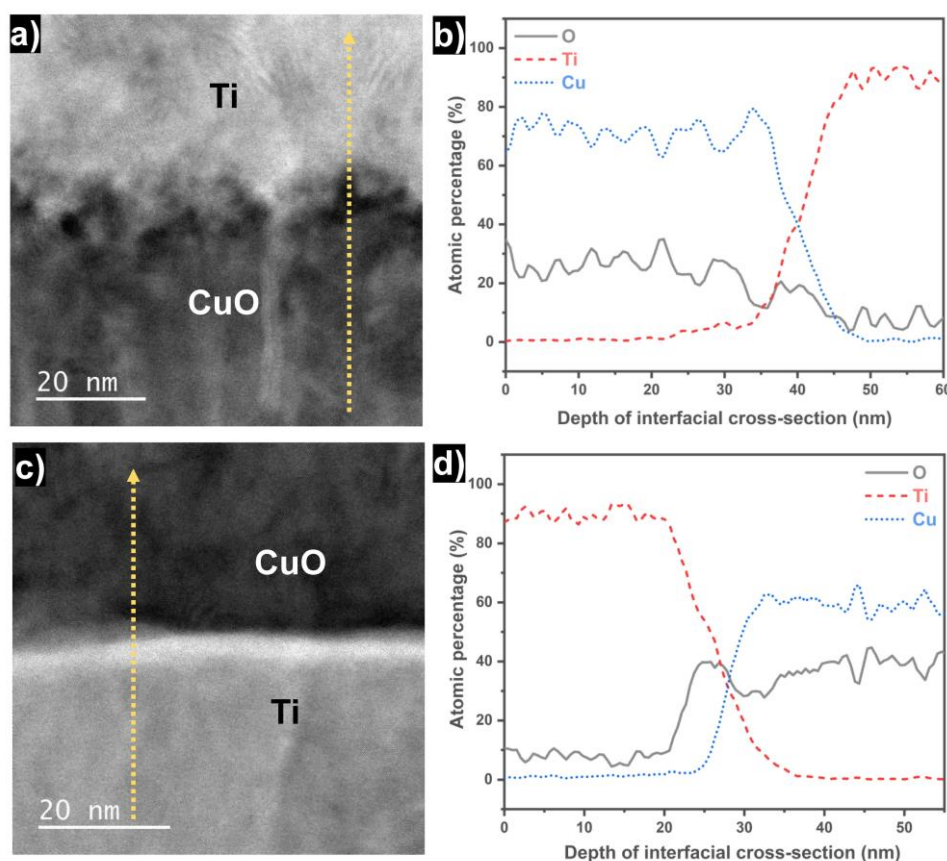
Figure 4. *HRTEM images (a and c) and EDX-line scan profiles (b and d) of CuO-Ti and Ti-CuO interfaces, respectively.*

From the chemical analysis standpoint, the CuO-Ti interface is ~12 nm long and consists of all three species. While Ti-CuO interface can be divided into two different sub-interfaces: the TiO interface in the first ~5 nm, followed by the intermixing of three species in the next 8 nm. It seems the roughness of the depositing surface plays an important role in the final composition of the interface. The rougher the surface, the more intermixing of three species. In addition, the copper oxide layer upon deposition of Ti features lower oxygen content than that of Al, indirectly implying titanium shows a higher reactivity in term of oxidation than aluminum, in consistency with the afore-discussed combustion performance and DSC results (**Fig. 2**).

3.2.2. Annealed

Fig. 5 and 6 present high magnification TEM cross-sections and EDX profiles of CuO-Ti, Ti-CuO interfaces and CuO/Ti/CuO/Al stack post the annealing treatment at 300 and 500 °C,

with a zoomed-in high-angle annular dark field (HAADF) image of Ti-CuO-Ti in **Fig. 6d**. For

comparison**, Fig. S9** presents high magnification TEM and EDX profile of CuO-Al post the

annealing treatment at 300 and 500 °C. Furthermore, the thicknesses of each layer (metal, fuel

and interfaces) measured from the TEM images (precision 1 nm) are reported in **Table 5**. As

the annealing temperature increases, both CuO-Ti and Ti-CuO interfaces grow (**Fig. 5)** and, the

CuO layers greatly modifies structurally, in thickness and composition (**Fig. 6c** and **Fig. 6d**).

Also, delamination was observed at both CuO-Ti and Ti-CuO interfaces (**Fig. 6b-c**) with lots

of high contrasted areas in between TiO_x layers and CuO, attributed to voids [38].

CuO-Ti interface: the CuO-Ti interface evolved from hardly distinguishable (as deposited) to

over a ~60 nm thick and well-define oxide layer after thermal annealing at 500 °C (**Fig. 5a** and

Fig. 5e). The atomic percentage ratio between Cu and O increased from 2 (as deposited) to 4

(annealed at 500 °C), which implies the CuO near the CuO-Ti interface has lost three quarters

of its oxygen content. Interestingly, the atomic percentage ratio of Ti to O at 500 °C equals to

1 (EDX profile of **Fig. 5f**) thus TiO is the proposed materials that develops in contact to CuO.

Due to the low sensitivity of EDX towards oxygen element, the exact oxidation state of titanium

in TiO_x will be further quantified in the EELS section.

Ti-CuO interface: the native titanium oxide layer at the Ti-CuO interface is thickening upon

annealing to reach ~ 65 nm thick after thermal treatment at 500 °C (**Fig. 5c** and **Fig. 5g**). The

atomic percentage ratio of Ti to O at 500 °C (EDX profile of **Fig. 5h** and **Fig. 6f**) indicate the

composition of TiO_2, and no more metallic Ti is present as the Ti layer contains ~20% of oxygen

(to be further examined by EELS) after thermal treatment at 500 °C. As a summary, from the

EDX analysis, confirmation is made that CuO starts to decompose at low temperature (300 °C)

to oxidize the adjacent titanium, which leads to the rapid growth of the titanium oxide interfacial

layer (more than 60 nm gain in thickness from ambient to 500 °C). Also, even deeper

penetration of oxygen atom throughout the initial titanium layer, beyond TiO and TiO_2 that are

grown upon annealing in their crystalline form, is consistent with the loss of the titanium XRD peak and oxygen presence from EDX spectra, at 500 °C.

Altogether these results not only support the DSC findings featuring a high exotherm event below 500 °C caused by the titanium oxidation, but also bring an explanation for the superior reactivity of CuO/Ti thermite over CuO/Al [33] linked to the stronger binding affinity of titanium with oxygen originated from CuO decomposition [39] and probable higher diffusion rate of oxygen through titanium oxide compared with aluminum oxide. Indeed, unlike CuO-Ti and Ti-CuO interfaces where oxygen penetrates deep inside the Ti layer after annealing to 500 °C, in CuO-Al and Al-CuO oxygen did not diffuse into the metallic aluminum layer: the oxygen signal drops to almost zero as passing through the alumina layer (see EDX line-scan through CuO-Al in **Fig. S9**). In addition, the aluminum oxide layer grows up to ~ 20 nm after annealing at 500 °C, against 60 nm for TiO_2 (**Table 5**), i.e. only one third.

CuO, Ti layers and Al/CuO/Ti/CuO. Interestingly, analyzing the CuO and Ti layer thickness variation upon annealing (**Table 5**), both the Ti and CuO do not vary much in thickness: a reduction of 26% and 10% only after the annealing at 500 °C, respectively, while the interfacial layer grows by 650%. As comparison, the aluminum layer does not change in thickness after annealing at 500 °C. The whole CuO/Ti/CuO/Al stack thickens by 7 %, corresponding to a ~50 nm global increase. This overall increase is consistent with the titanium oxidation: the ratio of density between pure Ti and rutile TiO_2 gives an estimate of ×1.82 increase of the titanium layering that is being oxidized, giving birth, in theory, to 74 nm of grown TiO_2. This reasonably falls in the order of magnitude of the experimentally grown titanium (~100 nm) as the estimate does not account for the lateral titanium over-density when turning titanium into TiO_2, that should lead to a slightly higher estimate.

The fast oxidation of atomic titanium by oxygen released from CuO decomposition leaves voids/delamination along the growing path (green dotted circles in **Fig. 6b**). EDX-line scans

inside these voids (L1 and L2, positions are highlighted in green in **Fig. 6d**) confirm that there are less materials in these triangle areas, especially with L2 position where the total atomic percentage drops to less than a half. Considering the EDX surface analysis can reach a sampling depth up to 100 nm, thus the line scan profile is in fact an accumulation of each element signals throughout a certain thickness of the examined layer.
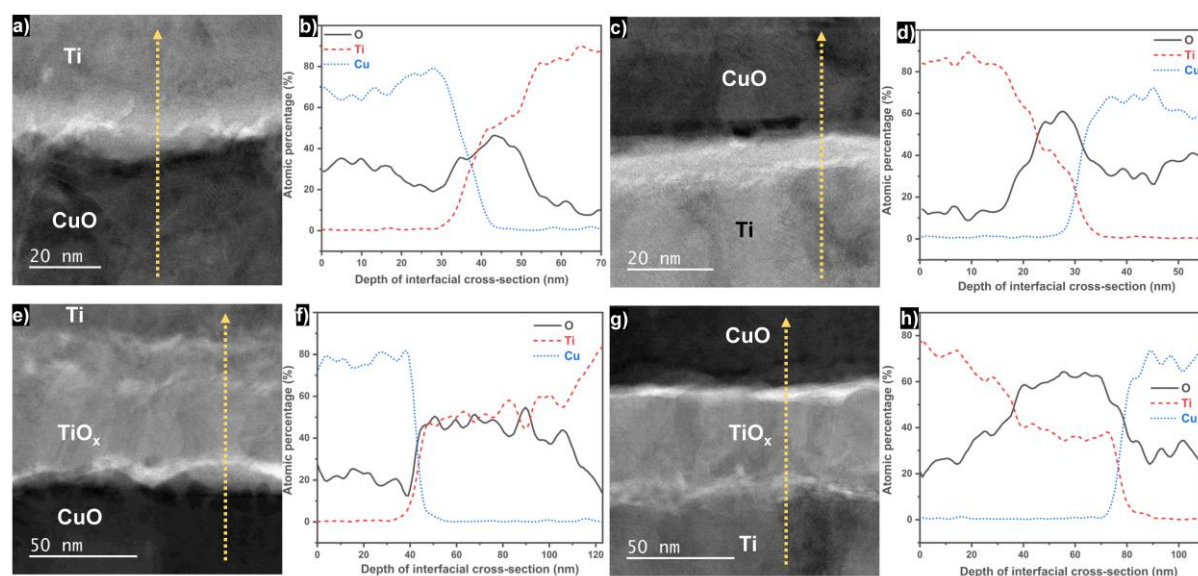

Figure 5. *STEM-EDX profile of each interfaces of CuO/Ti/CuO/Al annealed at 300 °C (a-d), and 500 °C (e-h).*
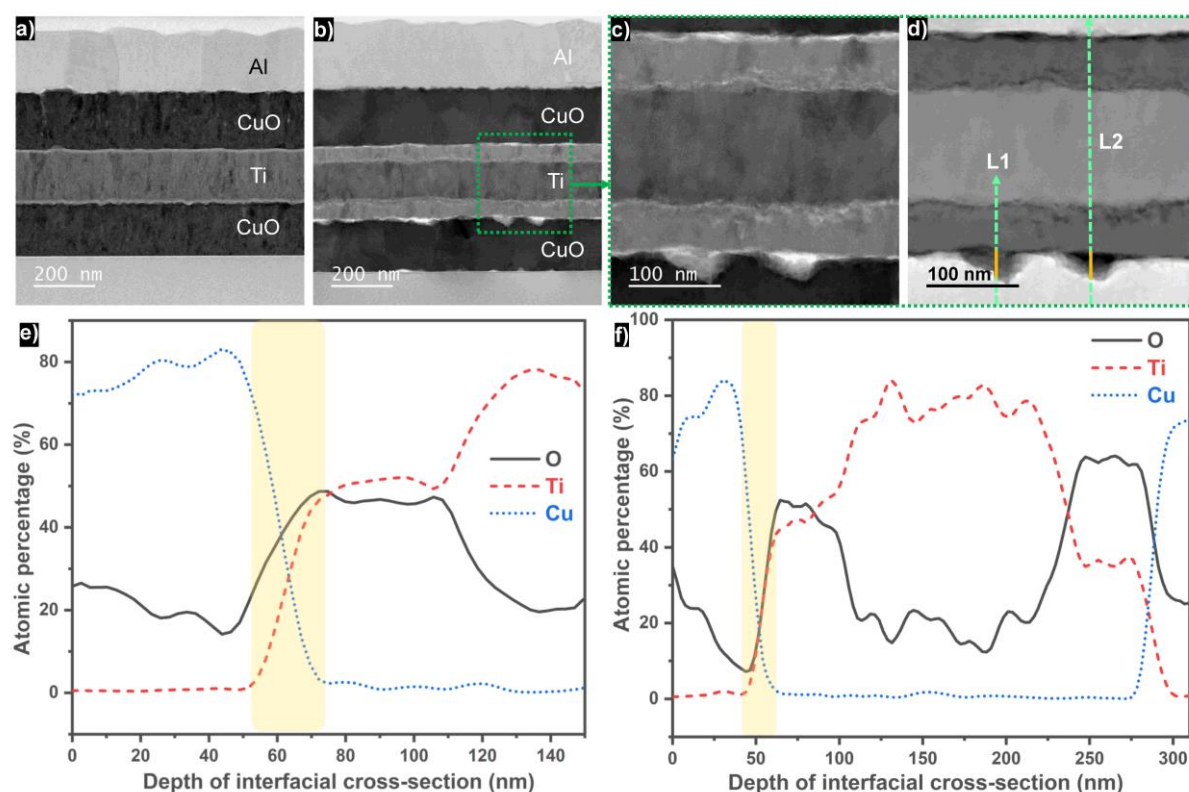
Figure 6. *STEM image of CuO/Ti/CuO/Al annealed at 300 °C (a) and 500 °C (b); zoomed-in STEM (c) and HAADF (d) images of CuO/Ti/CuO interfaces from sample annealed at 500 °C; EDX line scan profiles of CuO-Ti interface: L1(e) and L2 (f), highlighted in green arrows.*

Table 5. Layer thickness changes of CuO/Ti/CuO/Al at various temperatures.

Temperature	Measured thickness (nm)							
(°C)	CuO	**TiO$_x$**	**Ti**	**TiO$_x$**	CuO	Al$_x$O$_y$	Al	**All**
25	194 ± 1	9 ± 3	161 ± 2	5 ± 0	199 ± 2	6 ± 1	200 ± 2	773 ± 3
300	177 ± 3	15 ± 3	162 ± 2	10 ± 1	189 ± 2	11 ± 2	200 ± 2	768 ± 9
500	177 ± 2	65 ± 2	119 ± 5	63 ± 4	189 ± 2	18 ± 2	200 ± 2	826 ± 4

High resolution TEM-EDX analysis revealed that the titania, as Ti+CuO terminal oxide, is grown into the Ti layer from the self-diffusion of oxygens released by CuO decomposition into

the growing interfacial layer. As a final experiment STEM-EELS, were performed on both the

Ti-CuO and the CuO-Ti interfaces after annealing with the goal to quantify the evolution of the

oxidation state of Ti and Cu and therefore validate the single oxygen diffusion. Hence, the

energy loss near edge structure (ELNES) of Ti $L_{2,3}$-edges at 456-462 eV, O K-edge at 536 eV

and Cu $L_{2,3}$-edges at 931-951 eV were acquired across the various interfaces. EELS core loss

edges were background subtracted using a power law fit before being plotted.

3.3. Ti oxidation state upon annealing

ELNES of the Ti and O are shown in **Fig. 7** for both TiO_x layers annealed at 300° and 500

°C. When annealed at 500 °C (**Fig. 7c**), the two ELNE Ti $L_{2,3}$-edges at 456 - 462 eV are

subdivided into four peaks as a result of the strong crystal-field splitting of Ti^{4+} from the

surrounding oxygen atoms [40], accompany with the same subdivision of oxygen K-edge at

532 eV [41]. Such splitting is not observed in samples annealed at 300 °C (**Fig. 7a and Fig.

7b**), except for the minor subdivision EELS O-K edge from the upper TiO_x layer, which might

indicate the presence of Ti^{2+} and/or Ti^{3+} [42]. Thus, the oxidation state evolution of titanium in

upper TiO_x layer (Ti-CuO interface) confirms the previously discussed EDX line scan results

(**Fig. 4-6**), i.e., as annealing temperate increases, TiO_x evolved from TiO to TiO_2. However, as

for the bottom TiO_x layer (CuO-Ti interface), EELS results indicate the presence of TiO_2 while

EDX results (**Fig. 5-6**) refers to a Ti to O atomic ratio at 1. Considering the low sensitivity of

EDX towards lighter elements [43], EELS is more trusted when it comes to determine oxidation

states. Thus, both TiO_x interfacial layers undergo the same development as annealing

temperature increases. Noteworthy, no O-K edge is detected in the Ti layer when annealed at

300 °C as shown in **Fig. 7a and Fig. 7b**, which proves the ~10% atomic oxygen content

detected by EDX in the scans of **Fig. 5a and Fig. 5d** is a detection error. However, as annealing

temperature increases to 500 °C, strong O-K edges are found in all EELS spectra of the Ti layer, in alignment with the EDX result (**Fig. 5** indicating 20% of oxygen into the Ti) where atomic oxygen to titanium ratio increases from ~ 0.1 (as deposited and annealed at 300 °C) to > 0.25 (annealed at 500 °C).

Contrary to the high oxygen content in titanium layer, no discernable O-K edge was detected in aluminum layer even at 500 °C (**Fig. S10**) that confirms the higher affinity of Ti towards oxygen than Al as discussed earlier.

More interestingly, the gaseous O_2 pre-peak at 535 eV observed at the interfacial layers of CuO/Al multilayers annealed at 500 °C (**Fig. S10b**) [33,34], indicating that the oxidation of Al occur in both gaseous and condensed phase mechanisms, is totally absent in CuO/Ti. Only oxygen ions are detected by EELS (**Fig. 7c**) in TiO_x interfaces regardless of the annealing temperatures, so that it is possible to conclude that the oxidation of titanium is governed by condensed phase mechanism as previous studies argued [30,44]. Unlike the CuO/Al system, the much faster oxidation of titanium layer impedes the formation and storage of gaseous O_2 inside voids created at the CuO/Ti interfaces.
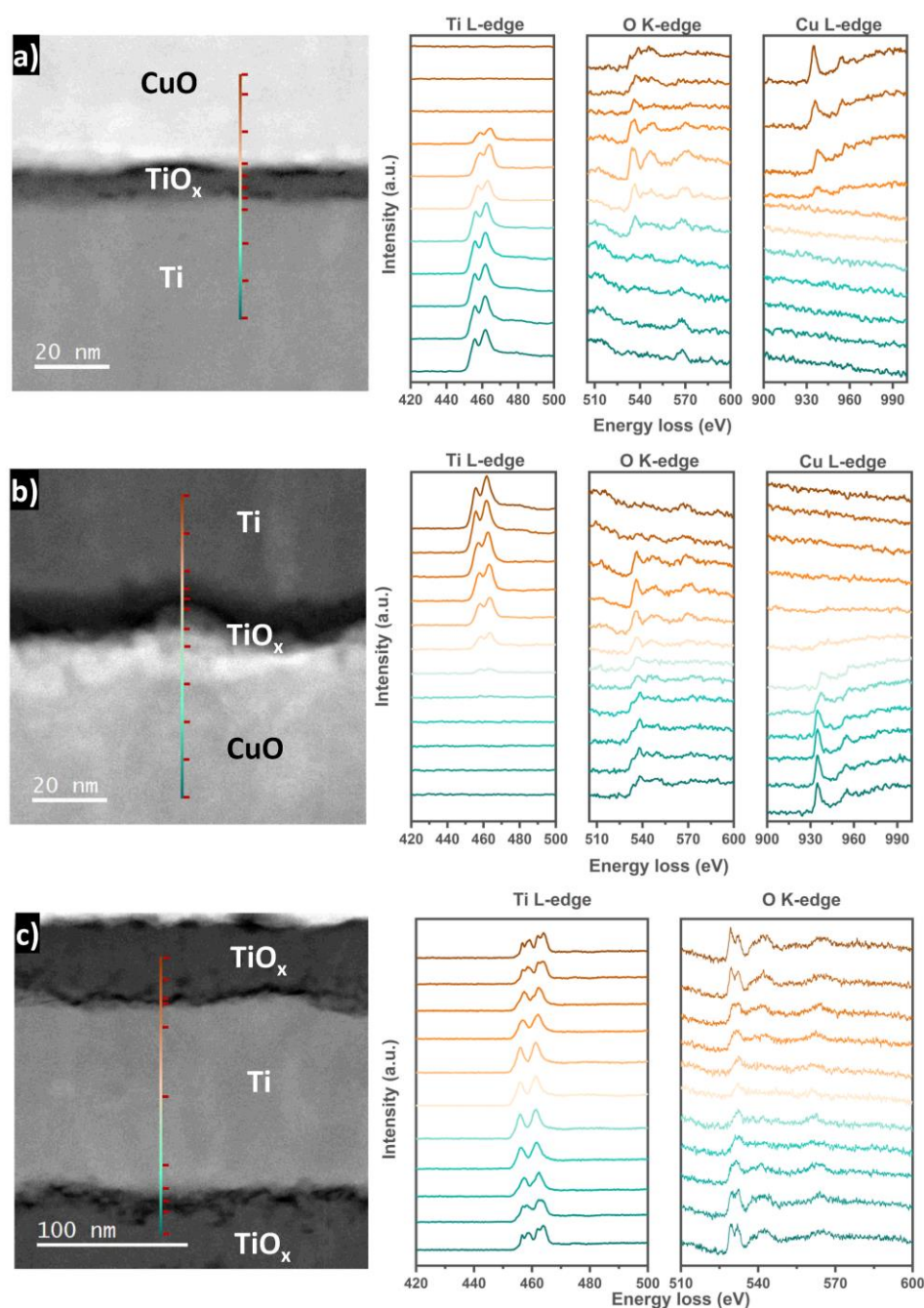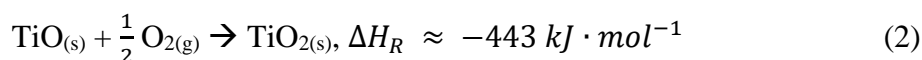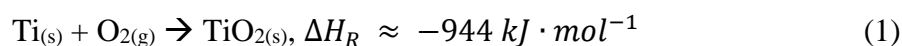
Figure 7. *STEM-HAADF-EELS results of Ti-CuO (a) and CuO-Ti (b) annealed at 300 °C, and TiO$_x$-Ti-TiO$_x$ annealed at 500 °C (c), showing Ti L$_{2,3}$, Cu L$_{2,3}$, and O k-edge.*

3.4. CuO/Ti reaction scenario

As for CuO/Al dense thermites, the early reduction of CuO when in contact with Ti has been evidenced by thermal analysis supported by TEM-EDX and STEM-EELS analyses. But, contrary to CuO/Al dense systems in which gaseous O$_2$ are detected at the reactants interface

at temperature as low as 350 °C [33], no gaseous O_2 are detected at the CuO/TiO_x interfaces despite numerous voids created upon annealing at 300 and 500 °C. Consistently, a titania interfacial layer is readily growing into the Ti layer to reach ~ 35% of its initial thickness at 500 °C.

Interestingly, two Ti oxidation states were observed by STEM-EELS analysis. At 300 °C, the Ti is oxidized into TiO (not detectable in XRD but quantified by STEM-EELS). At 500 °C, the TiO is further oxidized into crystalline TiO_2, and no more Ti is detected as being oxidized in TiO. Indeed, TiO_2, Cu_2O and Cu are detected by XRD without metallic Ti. This is consistent with DSC results featuring one single major exotherm located at ~ 430 °C generating the ~70% of the total heat of reaction. The second broad exotherm at 807 °C may correspond to the second oxidation step.

$$Ti_{(s)} + O_{2(g)} \rightarrow TiO_{2(s)}, \Delta H_R \approx -944 \; kJ \cdot mol^{-1} \qquad (1)$$

$$TiO_{(s)} + \frac{1}{2} O_{2(g)} \rightarrow TiO_{2(s)}, \Delta H_R \approx -443 \; kJ \cdot mol^{-1} \qquad (2)$$

Importantly, although the Al+CuO redox reaction in CuO/Al dense thermites is controlled by the diffusion of Al and slower counter diffusion of O through the growing alumina layer, only oxygens diffuse through the growing titania layer. In other words, Ti ions do not move which explain why no TiCu alloying was observed by contrast to Al_2Cu (endotherm at ~ 540 °C in DSC). Hence, the reaction occurs at the Ti/TiO_x interface, Ti and Cu remains always separated by a layer of TiO_x preventing formation of the alloys. The schematic diagram in **Fig. 8** shows the above discussed reaction in CuO/Ti fully dense thermites.
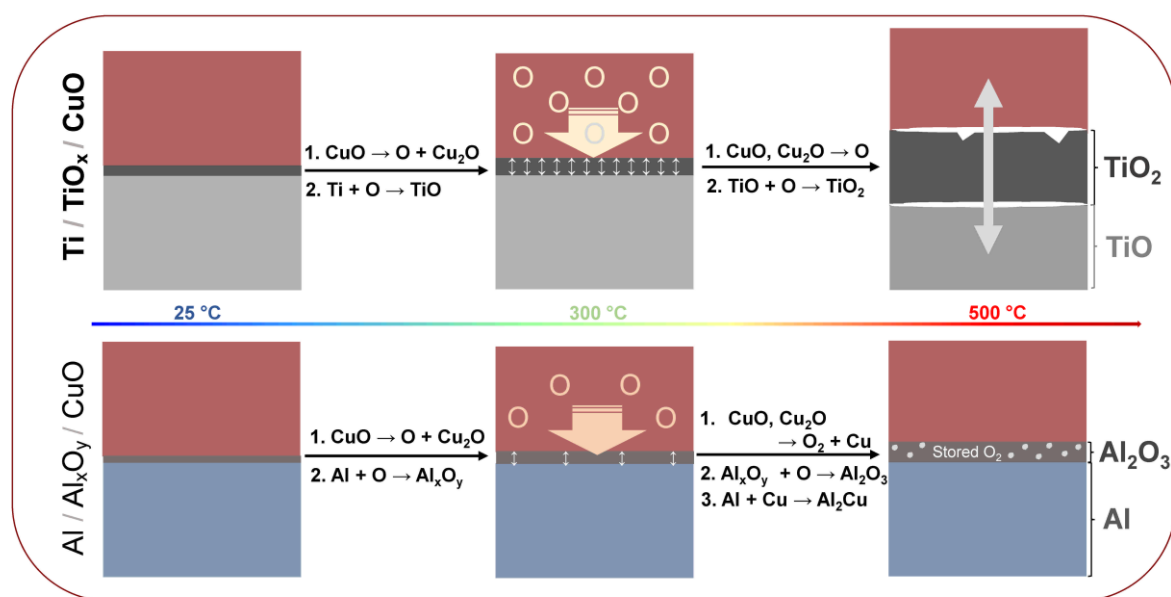
Figure 8. Schematic of the reaction mechanism of CuO/Ti compared with CuO/Al.

3.5. Improving ignitability of initiation chips by adding Ti into Al/CuO multilayers

   To take advantage of the high reactivity of CuO/Ti material, a thin layer of Ti was incorporated into the first CuO of Al/CuO stacks grown on ignition devices to test its influence. Compared to the commonly used CuO/Al$_{15BL}$ [34,35], the first few bilayers of CuO/Al was replaced by CuO/Ti and referred as (CuO/Ti)$_{xBL}$/(CuO/Al)$_{(15-x)BL}$, x equal to 0, 1, 2 or 3. (CuO/Ti)$_{1BL}$/(CuO/Al)$_{14BL}$ means that only one CuO/Ti bilayer is deposited followed by the deposition of 14 bilayers of CuO/Al. For all the samples, the thicknesses of CuO, Ti and Al were set to 200 nm, 170 nm and 200 nm, respectively. The ignition delay of (CuO/Ti)$_{xBL}$/(CuO/Al)$_{(15-x)BL}$ reduced by almost an order of magnitude, from more than 15 ms to less than 0.3 ms as the number of CuO/Ti bilayer increases from 0 to 3. Interestingly, the beneficial effect of CuO/Ti reaches a plateau as the number of CuO/Ti bilayers is ≥ 2. Only replacing the first 2 CuO/Al bilayers with CuO/Ti can maximumly improve the overall ignition performance.
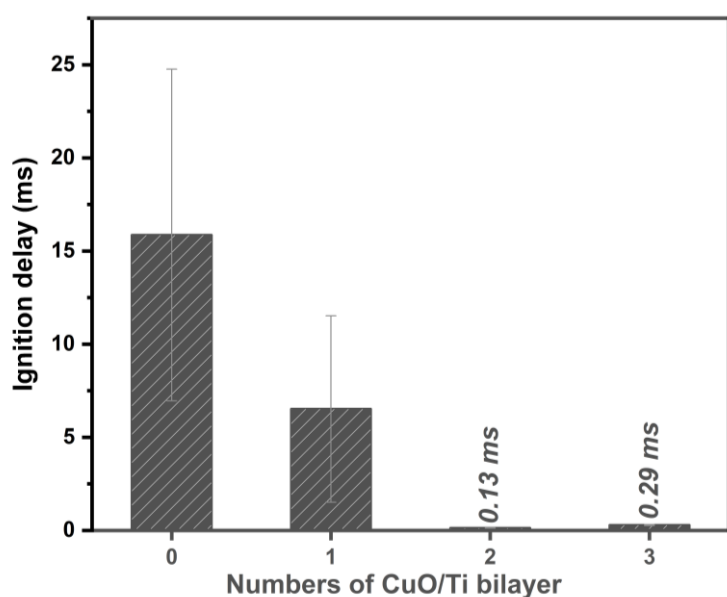
Figure 9. *Ignition delay of (CuO/Ti)$_{xBL}$/(CuO/Al)$_{(15-x)BL}$ nanolaminates (x =0, 1, 2, or 3).*

CONCLUSIONS

In this work, magnetron-sputtered CuO/Ti multilayers were prepared by magnetron sputtering

and characterized to assess their ignition point and reactivity. The as-prepared CuO/Ti

nanothermites ignite much sooner (ignition energy reduction by 5) and burn faster (burn rate

enhancement ×3) compared to equivalent CuO/Al material. Atomically resolved

STEM−HAADF, HRTEM-EDX and STEM−EELS were then performed on partially reacted

CuO/Ti multilayers to understand the mechanisms leading to the superior reactivity and

ignitability of Ti based nanothermites. Results show that the Ti has a better affinity with oxygen

than Al: ~70% of the total heat of reaction of the Ti/CuO system is released within a single

exotherm at 430 °C, against only 30% for Al/CuO system. Also, in CuO/Ti, solely oxygen

atoms migrate through the titania layer to react with Ti at the TiO$_2$/Ti interface, contrary to the

dual O and Al migration observed in CuO/Al one. As a consequence, titania grows and

propagates into the Ti layer and no Ti/Cu alloying occurs during the reaction, which is another difference with the Al_2Cu formation seen in CuO/Al system. Finally, Ti+CuO redox reaction undergoes a two-step oxidation process: at 300 °C, Ti is first oxidized into TiO and further oxidized into crystalline TiO_2 at 500 °C. This study confirms that Ti can be of great interest in addition of Al in nanothermites, for applications where it is desirable to lower the ignition temperature. Adding two CuO/Ti bilayers prior to the deposition of CuO/Al multilayers allows reaching ignition delays below the ms regime (ignition time of 200 µs) against 15 ms without CuO/Ti.

Funding Sources

Declaration of Competing Interests

The authors declare that they have no known competing financial interests or personal relationships that could have appeared to influence the work reported in this paper.

Acknowledgements

Appendix A. Supplementary data

Supplementary data to this article can be found online at …

REFERENCES

[1]   L.L. Wang, Z.A. Munir, Y.M. Maximov, Thermite reactions: their utilization in the synthesis and processing of materials, Journal of Materials Science. 28 (1993) 3693–3708. https://doi.org/10.1007/BF00353167.

[2]   C.L. Yeh, Y.S. Huang, Thermite reduction of Ta2O5/SiO2 powder mixtures for combustion synthesis of Ta-based silicides, Journal of Alloys and Compounds. 509 (2011) 6302–6306. https://doi.org/10.1016/j.jallcom.2011.03.063.

[3]   M.J. Abere, M.T. Beason, R.V. Reeves, M.A. Rodriguez, P.G. Kotula, C.E. Sobczak, S.F. Son, C.D. Yarrington, D.P. Adams, The growth and nanothermite reaction of 2Al/3NiO multilayer thin films, Journal of Applied Physics. 132 (2022) 035305. https://doi.org/10.1063/5.0096787.

[4]   D.M.B. Dombroski, A. Wang, J.Z. Wen, M. Alfano, Joining and welding with a nanothermite and exothermic bonding using reactive multi-nanolayers – A review, Journal of Manufacturing Processes. 75 (2022) 280–300. https://doi.org/10.1016/j.jmapro.2021.12.056.

[5]   A.H. Kinsey, K. Slusarski, S. Sosa, T.P. Weihs, Gas Suppression via Copper Interlayers in Magnetron Sputtered Al–Cu2O Multilayers, ACS Appl. Mater. Interfaces. 9 (2017) 22026–22036. https://doi.org/10.1021/acsami.7b03071.

[6]   H. Sui, N. Huda, Z. Shen, J.Z. Wen, Al–NiO energetic composites as heat source for joining silicon wafer, Journal of Materials Processing Technology. 279 (2020). https://doi.org/10.1016/j.jmatprotec.2019.116572.

[7]   J. Xu, Y. Tai, Y. Shen, J. Dai, W. Xu, Y. Ye, R. Shen, Y. Hu, Characteristics of energetic semiconductor bridge initiator based on different stoichiometric ratios of Al/MoO3 reactive multilayer films under capacitor discharge conditions, Sensors and Actuators A: Physical. 296 (2019) 241–248. https://doi.org/10.1016/j.sna.2019.07.015.

[8]   R.R. Nellums, S.F. Son, L.J. Groven, Preparation and Characterization of Aqueous Nanothermite Inks for Direct Deposition on SCB Initiators, Propellants, Explosives, Pyrotechnics. 39 (2014) 463–470. https://doi.org/10.1002/prep.201400013.

[9]   L. Glavier, A. Nicollet, F. Jouot, B. Martin, J. Barberon, L. Renaud, C. Rossi, Nanothermite/RDX-Based Miniature Device for Impact Ignition of High Explosives, Propellants, Explosives, Pyrotechnics. 42 (2017) 308–317. https://doi.org/10.1002/prep.201600154.

[10] A. Nicollet, L. Salvagnac, V. Baijot, A. Estève, C. Rossi, Fast circuit breaker based on integration of Al/CuO nanothermites, Sensors and Actuators A: Physical. 273 (2018) 249–255. https://doi.org/10.1016/j.sna.2018.02.044.

[11] S.S. Pandey, N. Banerjee, Y. Xie, C.H. Mastrangelo, Self-Destructing Secured Microchips by On-Chip Triggered Energetic and Corrosive Attacks for Transient Electronics, Advanced Materials Technologies. 3 (2018) 1800044. https://doi.org/10.1002/admt.201800044.

[12] C.S. Staley, K.E. Raymond, R. Thiruvengadathan, S.J. Apperson, K. Gangopadhyay, S.M. Swaszek, R.J. Taylor, S. Gangopadhyay, Fast-Impulse Nanothermite Solid-Propellant Miniaturized Thrusters, Journal of Propulsion and Power. 29 (2013) 1400–1409. https://doi.org/10.2514/1.B34962.

[13] M. H. Ervin, S. S. Bedair, C. R. Knick, H. Tsang, B. Isaacson, N. W. Piekiel, Evaporation Driven Assembly of On-Chip Thermite Devices, Journal of

Microelectromechanical Systems. 26 (2017) 1408–1416.
https://doi.org/10.1109/JMEMS.2017.2757149.

[14] A. Williams, I. Shancita, I. Altman, N. Tamura, M.L. Pantoya, On the Pressure Generated by Thermite Reactions Using Stress-Altered Aluminum Particles, Propellants, Explosives, Pyrotechnics. 46 (2021) 99–106. https://doi.org/10.1002/prep.202000221.

[15] T. Wu, G. Lahiner, C. Tenailleau, B. Reig, T. Hungria, A. Esteve, C. Rossi, Unexpected Enhanced Reactivity of Aluminized Nanothermites by Accelerated Aging, Chemical Engineering Journal. (2021) 129432. https://doi.org/10.1016/j.cej.2021.129432.

[16] P. Biswas, F. Xu, P. Ghildiyal, M.R. Zachariah, In-Situ Thermochemical Shock-Induced Stress at the Metal/Oxide Interface Enhances Reactivity of Aluminum Nanoparticles, ACS Appl. Mater. Interfaces. 14 (2022) 26782–26790. https://doi.org/10.1021/acsami.2c05412.

[17] B. Julien, P. Dubreuil, C. Josse, L. Salvagnac, S. Pelloquin, A. Esteve, C. Rossi, Effect of substrate–induced localized stress on the combustion properties of Al/CuO reactive multilayer films, Thin Solid Films. 740 (2021) 139000. https://doi.org/10.1016/j.tsf.2021.139000.

[18] W. He, W. Ao, G. Yang, Z. Yang, Z. Guo, P.-J. Liu, Q.-L. Yan, Metastable energetic nanocomposites of MOF-activated aluminum featured with multi-level energy releases, Chemical Engineering Journal. 381 (2020) 122623. https://doi.org/10.1016/j.cej.2019.122623.

[19] W. He, Z.-H. Li, S. Chen, G. Yang, Z. Yang, P.-J. Liu, Q.-L. Yan, Energetic metastable n-Al@PVDF/EMOF composite nanofibers with improved combustion performances, Chemical Engineering Journal. 383 (2020) 123146. https://doi.org/10.1016/j.cej.2019.123146.

[20] D.-Y. Tang, J. Lyu, W. He, J. Chen, G. Yang, P.-J. Liu, Q.-L. Yan, Metastable intermixed Core-shell Al@M(IO3)x nanocomposites with improved combustion efficiency by using tannic acid as a functional interfacial layer, Chemical Engineering Journal. 384 (2020) 123369. https://doi.org/10.1016/j.cej.2019.123369.

[21] T. Wu, X. Wang, J.B. DeLisio, S. Holdren, M.R. Zachariah, Carbon addition lowers initiation and iodine release temperatures from iodine oxide-based biocidal energetic materials, Carbon. 130 (2018) 410–415. https://doi.org/10.1016/j.carbon.2018.01.001.

[22] J.B. DeLisio, X. Hu, T. Wu, G.C. Egan, G. Young, M.R. Zachariah, Probing the Reaction Mechanism of Aluminum/Poly(vinylidene fluoride) Composites, J. Phys. Chem. B. 120 (2016) 5534–5542. https://doi.org/10.1021/acs.jpcb.6b01100.

[23] L. Marín, Y. Gao, M. Vallet, I. Abdallah, B. Warot-Fonrose, C. Tenailleau, A.T. Lucero, J. Kim, A. Esteve, Y.J. Chabal, C. Rossi, Performance Enhancement via Incorporation of ZnO Nanolayers in Energetic Al/CuO Multilayers, Langmuir. 33 (2017) 11086–11093. https://doi.org/10.1021/acs.langmuir.7b02964.

[24] X. Liu, K.-L. Chintersingh, M. Schoenitz, E.L. Dreizin, Reactive Composite Boron–Magnesium Powders Prepared by Mechanical Milling, Journal of Propulsion and Power. 34 (2018) 787–794. https://doi.org/10.2514/1.B36315.

[25] W. Zhao, H. Wang, D.J. Kline, X. Wang, T. Wu, J. Xu, H. Ren, M.R. Zachariah, Influence of titanium addition on performance of boron-based thermites, Chemical Engineering Journal. 438 (2022) 134837. https://doi.org/10.1016/j.cej.2022.134837.

[26] X. Wang, T. Wu, H. Wang, J.B. DeLisio, Y. Yang, M.R. Zachariah, Boron ignition and combustion with doped δ-Bi2O3: Bond energy/oxygen vacancy relationships, Combustion and Flame. 197 (2018) 127–133. https://doi.org/10.1016/j.combustflame.2018.07.015.

[27] W. Zhao, H. Ren, T. Yan, Y. Ou, Q. Jiao, H. Wang, D.J. Kline, M.R. Zachariah, Tailoring energy release of nano-Si based thermites via incorporation of Ti

nanoparticles, Chemical Engineering Journal. 396 (2020) 124559.
https://doi.org/10.1016/j.cej.2020.124559.

[28] C. Wei, J. Wei, L. Pingyun, L. Li, C. Binhua, D. Junjun, W. Longxiang, Y. Yuan, L. Fengsheng, Ignition and Combustion of Super-Reactive Thermites of AlMg/KMnO4, Rare Metal Materials and Engineering. 42 (2013) 2458–2461. https://doi.org/10.1016/S1875-5372(14)60038-2.

[29] Y. Aly, M. Schoenitz, E.L. Dreizin, Aluminum-Metal Reactive Composites, Null. 183 (2011) 1107–1132. https://doi.org/10.1080/00102202.2011.584090.

[30] W. Zhao, X. Wang, H. Wang, T. Wu, D.J. Kline, M. Rehwoldt, H. Ren, M.R. Zachariah, Titanium enhanced ignition and combustion of Al/I2O5 mesoparticle composites, Combustion and Flame. 212 (2020) 245–251. https://doi.org/10.1016/j.combustflame.2019.04.049.

[31] Y.L. Shoshin, E.L. Dreizin, Particle combustion rates for mechanically alloyed Al–Ti and aluminum powders burning in air, Combustion and Flame. 145 (2006) 714–722. https://doi.org/10.1016/j.combustflame.2005.11.006.

[32] L. Salvagnac, S. Assie-Souleille, C. Rossi, Layered Al/CuO Thin Films for Tunable Ignition and Actuations, Nanomaterials. 10 (2020). https://doi.org/10.3390/nano10102009.

[33] V. Singh, B. JULIEN, L. Salvagnac, S. Pelloquin, T. Hungria, C. Josse, M. Belhaj, C. Rossi, Influence of process parameters on energetic properties of sputter-deposited Al/CuO reactive multilayers, Nanotechnology. (2022). http://iopscience.iop.org/article/10.1088/1361-6528/ac85c5.

[34] B. Julien, J. Cure, L. Salvagnac, C. Josse, A. Esteve, C. Rossi, Integration of Gold Nanoparticles to Modulate the Ignitability of Nanothermite Films, ACS Appl. Nano Mater. 3 (2020) 2562–2572. https://doi.org/10.1021/acsanm.9b02619.

[35] T. Wu, B. Julien, H. Wang, S. Pelloquin, A. Esteve, M.R. Zachariah, C. Rossi, Engineered Porosity-Induced Burn Rate Enhancement in Dense Al/CuO Nanothermites, ACS Appl. Energy Mater. 5 (2022) 3189–3198. https://doi.org/10.1021/acsaem.1c03805.

[36] I. Abdallah, J. Zapata, G. Lahiner, B. Warot-Fonrose, J. Cure, Y. Chabal, A. Esteve, C. Rossi, Structure and Chemical Characterization at the Atomic Level of Reactions in Al/CuO Multilayers, ACS Appl. Energy Mater. 1 (2018) 1762–1770. https://doi.org/10.1021/acsaem.8b00296.

[37] M. Mursalat, C. Huang, B. Julien, M. Schoenitz, A. Esteve, C. Rossi, E.L. Dreizin, Low-Temperature Exothermic Reactions in Al/CuO Nanothermites Producing Copper Nanodots and Accelerating Combustion, ACS Appl. Nano Mater. 4 (2021) 3811–3820. https://doi.org/10.1021/acsanm.1c00236.

[38] Y.-C. Kim, J. Kim, J.-H. Choy, J.-C. Park, H.-M. Choi, Effects of cobalt silicidation and postannealing on void defects at the sidewall spacer edge of metal–oxide–silicon field-effect transistors, Appl. Phys. Lett. 75 (1999) 1270–1272. https://doi.org/10.1063/1.124664.

[39] T.H. Okabe, C. Zheng, Y. Taninouchi, Thermodynamic Considerations of Direct Oxygen Removal from Titanium by Utilizing the Deoxidation Capability of Rare Earth Metals, Metallurgical and Materials Transactions B. 49 (2018) 1056–1066. https://doi.org/10.1007/s11663-018-1172-4.

[40] C.-N. Huang, J.-S. Bow, Y. Zheng, S.-Y. Chen, N. Ho, P. Shen, Nonstoichiometric Titanium Oxides via Pulsed Laser Ablation in Water, Nanoscale Research Letters. 5 (2010) 972. https://doi.org/10.1007/s11671-010-9591-4.

[41] R. Brydson, B.G. Williams, W. Engel, H. Sauer, E. Zeitler, J.M. Thomas, Electron energy-loss spectroscopy (EELS) and the electronic structure of titanium dioxide, Solid

State Communications. 64 (1987) 609–612. https://doi.org/10.1016/0038-1098(87)90792-7.

[42] B. Cao, K. Suenaga, T. Okazaki, H. Shinohara, Production, Isolation, and EELS Characterization of Ti2@C84 Dititanium Metallofullerenes, J. Phys. Chem. B. 106 (2002) 9295–9298. https://doi.org/10.1021/jp026013b.

[43] A. Lazzarini, M. Crucianelli, Chemical characterization of extraterrestrial sample return: a versatile platform @UnivAQ, Memorie Della Societa Astronomica Italiana. 92 (2021) 166.

[44] M.C. Rehwoldt, Y. Yang, H. Wang, S. Holdren, M.R. Zachariah, Ignition of Nanoscale Titanium/Potassium Perchlorate Pyrotechnic Powder: Reaction Mechanism Study, J. Phys. Chem. C. 122 (2018) 10792–10800. https://doi.org/10.1021/acs.jpcc.8b03164.